

RESEARCH ARTICLE

10.1029/2018JC014102

The Relationship of Near-Surface Flow, Stokes Drift and the Wind Stress

Allan J. Clarke¹  and Stephen Van Gorder¹ ¹Department of Earth, Ocean and Atmospheric Science, Florida State University, Tallahassee, FL, USA

Key Points:

- Based on analysis of in situ ocean observations, on average Stokes drift is driven by the local wind, and is in the direction of the wind
- The *e*-folding decay depth of the Stokes drift is typically less than 1.8 m and so Stokes drift is not canceled by an induced Eulerian flow
- Stokes drift speed is strongly dependent on high-frequency waves having frequencies less than a wave break frequency

Correspondence to:

A. J. Clarke,
aclarke@fsu.edu

Citation:

Clarke, A. J., & Van Gorder, S. (2018). The relationship of near-surface flow, Stokes drift, and the wind stress. *Journal of Geophysical Research: Oceans*, 123, 4680–4692. <https://doi.org/10.1029/2018JC014102>

Received 23 APR 2018

Accepted 5 JUN 2018

Accepted article online 12 JUN 2018

Published online 5 JUL 2018

Abstract Many years of simultaneous hourly buoy wind and directional wave spectra data in the Gulf of Mexico and the Pacific were used to estimate Stokes drift and $u_* \mathbf{e}_w$ where $u_* = (\text{magnitude of the local windstress/water density})^{1/2}$ and \mathbf{e}_w is a unit vector in the direction of the local wind. Stokes drift and $u_* \mathbf{e}_w$ were strongly vectorially correlated, the two vectors on average being within a few degrees of one another. This result remained valid even when there was evidence of remotely forced swell. Extension of the observed wave spectra above 0.35 Hz to the u_* -dependent wave breaking frequency shows that typically the *e*-folding scale of the Stokes drift with depth is less than 1.8 m, much smaller than the Ekman layer *e*-folding scale. Therefore, there is negligible induced Eulerian cancellation of the Stokes drift, and the surface particle movement is governed by the Eulerian velocity + $|\mathbf{u}_{\text{Stokes}}| \mathbf{e}_w$. Taking into account wave spreading, $|\mathbf{u}_{\text{Stokes}}|$ typically ranges from about 3 to 13 cm/s. Thus, the Stokes drift, which can be estimated directly from the wind stress, is an order one contributor to the surface transport of particles.

Plain Language Summary Although crucial for the movement of oil spills, red tide, fish eggs and larvae, and floating garbage, much still has to be learned about net particle movement in the top 1 or 2 m of the ocean. George Gabriel Stokes showed mathematically in 1847 that ocean surface waves may affect the net movement of particles at the ocean surface, but later it was shown that because we live on a rotating Earth, the net particle movement in the direction of the waves (the “Stokes drift”) might be canceled by another opposite flow. In this paper we demonstrate that because of the ocean turbulence generated by the wind, the main part of the Stokes drift in the top 2 m of the ocean is not canceled by an opposing flow. Furthermore, analysis of simultaneous hourly wind and wave measurements for many years at Christmas Island in the equatorial Pacific, ocean station Papa in the north Pacific, and 10 stations in the Gulf of Mexico shows that Stokes drift is strongly related to the local wind and is in the direction of the wind. Stokes drift is therefore not primarily due to remotely driven swell; rather, it is mainly due to the much shorter waves that the local wind generates. By taking into account when the short waves break, it is shown how Stokes drift can be approximately estimated directly from the local wind.

1. Introduction

Over the last few decades it has become increasingly apparent that surface gravity waves play a key role in upper-ocean mixing and the near-surface Lagrangian movement of particles via Stokes drift (see, e.g., the review by van den Bremer & Breivik, 2018). We have known about Stokes drift since the nineteenth century when Stokes (1847) mathematically established the existence of such a “drift” of particles in the direction of wave propagation. Although much is known about wind-generated waves, much less is known about the relationship of Stokes drift to the local wind and to the near-surface movement of particles in the real ocean.

It has been recognized (see, e.g., Tamura et al., 2012; Webb & Fox-Kemper, 2011) that since Stokes drift is proportional to frequency cubed, its magnitude depends strongly on the high-frequency tail of the spectrum. However, so far, it has been unclear how to calculate the Stokes drift, because a justification of how to limit the high-frequency contribution has not been given. In section 5 we offer a physical argument, backed by observations, for how this might be done.

But before doing this we discuss two other ways that the inclusion of the high-frequency tail is crucial to the dynamics. First, in section 2, we apply the theory of McWilliams et al. (1997) and Polton et al. (2005) to show that whether the Stokes drift affects the near-surface Lagrangian flow *at all* depends on the relative size of δ_{Stokes} , the vertical decay scale of the Stokes drift, to δ_{Ek} , the Ekman layer *e*-folding scale. Only if this ratio is small will Stokes drift not be canceled by an induced Eulerian flow, and the size of this ratio is strongly influenced by the high-frequency spectral tail. Second, in section 4, we show, using simultaneous hourly

wind and directional spectra observations in the Gulf of Mexico and the Pacific, that Stokes drift is essentially driven by the local wind and is in the local wind direction. This is true even when, as in the case of Christmas Island, the wave spectrum clearly indicates the presence of remotely driven swell.

2. Stokes Drift Background

For a surface gravity wave of angular frequency ω , wave number k , and amplitude a the sea level can be represented as

$$\eta = a \cos(ks - \omega t), \quad (1)$$

where s is the distance along the direction of wave propagation. To an excellent approximation relevant water depths are large enough to limit our analysis to deepwater gravity waves. In that case, for small ka , the Stokes drift $\mathbf{u}_{\text{Stokes}}$ for the sea level of amplitude a is

$$\mathbf{u}_{\text{Stokes}} = a^2 \omega^3 g^{-1} \exp(2kz) \mathbf{e}_{\text{wave}}. \quad (2)$$

where g is the acceleration due to gravity, z is distance upward from the ocean surface at rest, and \mathbf{e}_{wave} is the unit vector in the direction of wave propagation.

Notice that since Stokes drift is a steady flow, in practice the rotation of the Earth must be taken into account. From an Eulerian point of view, Hasselmann (1970) showed that when the Coriolis force is taken into account, the horizontal wave velocity vector is not exactly 90° out of phase with the vertical velocity vector as it is in the nonrotating system, and the Reynolds stress term due to the waves gives rise to a mean acceleration $-\mathbf{f} \mathbf{e}_3 \times \mathbf{u}_{\text{Stokes}}$, where f is the Coriolis parameter and \mathbf{e}_3 is the unit vertical vector. When this ‘‘Coriolis-Stokes’’ acceleration is included in the classical Ekman layer problem, we have

$$f \mathbf{e}_3 \times \mathbf{u} = -f \mathbf{e}_3 \times \mathbf{u}_{\text{Stokes}} + \frac{\partial \tau}{\partial z} / \rho, \quad (3)$$

where \mathbf{u} is the time-averaged horizontal (Eulerian) velocity, ρ is the water density, and τ is the turbulent stress in the water. Notice that when there is no turbulent stress, $\partial \tau / \partial z = 0$, and (3) has a solution $\mathbf{u} = -\mathbf{u}_{\text{Stokes}}$, that is, the time mean particle velocity $\mathbf{u} + \mathbf{u}_{\text{Stokes}} = 0$. In other words, when there is no mixing or turbulence in the quasi-steady dynamics of (3), the Coriolis-Stokes acceleration induces a time-averaged Eulerian current that exactly cancels the Stokes drift so that, consistent with Ursell (1950) and Pollard (1970), there is no net particle displacement. However, in the usual case in the real ocean when turbulent stress is present, the cancellation does not occur and, in fact, calculations suggest that the surface mean particle drift is dominated by the Stokes drift (McWilliams et al., 2012).

Using theory reported by McWilliams et al. (1997) and Polton et al. (2005), we can understand the main features of the influence of turbulent stress on the Stokes drift by considering the simple case when the turbulent stress is represented using a constant eddy viscosity κ so that in (3)

$$\frac{\partial \tau}{\partial z} / \rho = \kappa \frac{\partial^2 \mathbf{u}}{\partial z^2}. \quad (4)$$

Substitution of (4) into (3) and then writing the equations in component form gives

$$-fv = fv_{\text{Stokes}} + \kappa \frac{\partial^2 u}{\partial z^2}, \quad (5)$$

$$fu = -fu_{\text{Stokes}} + \kappa \frac{\partial^2 v}{\partial z^2}. \quad (6)$$

In standard fashion the Ekman problem is most easily solved by writing

$$w = u + iv, \quad (7)$$

and noting that (5) and (6) are the real and imaginary parts of

$$\kappa w_{zz} - iw = iw_{\text{Stokes}}. \quad (8)$$

Since $\kappa = f\delta_{\text{Ek}}^2/2$ where δ_{Ek} is the Ekman layer decay scale, (8) can also be written as

$$w_{zz} - 2iw/\delta_{\text{Ek}}^2 = 2iw_{\text{Stokes}}/\delta_{\text{Ek}}^2. \quad (9)$$

At the surface w satisfies the stress boundary condition that

$$\rho\kappa w_z = \tau_0^x + i\tau_0^y = \tau_0 \quad \text{at } z = 0, \quad (10)$$

where τ_0^x and τ_0^y are the x and y components of the wind stress. The velocity w also satisfies $w \rightarrow 0$ as $z \rightarrow -\infty$ because we limit our analysis to water deeper than δ_{Ek} and δ_{Stokes} , the vertical decay scale of the Stokes drift.

The Stokes drift decays exponentially with depth for a single frequency, and temporarily we focus on this case. The results for the whole spectrum can be found by summing the single-frequency results. We write

$$w_{\text{Stokes}} = w_{\text{Stokes}}(0) \exp(z/\delta_{\text{Stokes}}). \quad (11)$$

The solution of (9) and its boundary conditions is

$$w = 2i\varepsilon^2 w_{\text{Stokes}}/(1 - 2i\varepsilon^2) + A \exp[(1 + i)z/\delta_{\text{Ek}}], \quad (12)$$

where

$$\varepsilon = \delta_{\text{Stokes}}/\delta_{\text{Ek}} \quad (13)$$

and

$$A = \frac{\tau_0(1 - i)}{\rho f \delta_{\text{Ek}}} - \frac{\varepsilon(1 + i)w_{\text{Stokes}}(0)}{1 - 2i\varepsilon^2}. \quad (14)$$

At the surface the net Lagrangian velocity w_{Lag} is given by

$$w_{\text{Lag}}(0) = w(0) + w_{\text{Stokes}}(0) = 2i\varepsilon^2 w_{\text{Stokes}}(0)/(1 - 2i\varepsilon^2) + A + w_{\text{Stokes}}(0). \quad (15)$$

From (14) and (15) we thus have that for small ε

$$w_{\text{Lag}}(0) = \tau_0(1 - i)/(\rho f \delta_{\text{Ek}}) + w_{\text{Stokes}}(0), \quad (16)$$

i.e., provided ε is small; the net surface Lagrangian flow is equal to the classical Ekman Eulerian flow plus the Stokes drift.

Using a third-generation wave model and hence a spectrum of waves, Tamura et al. (2012) showed that the mean Stokes drift e -folding depth in the Pacific north of 30°S is 1–2 m. Our Pacific calculations agree with Tamura et al. and for the Gulf of Mexico (see section 7) give even smaller δ_{Stokes} (see Figure 6). All these values for δ_{Stokes} are much smaller than δ_{Ek} , so ε is small. Consequently, when turbulence is taken into account, the Stokes drift is not canceled by an induced-Eulerian flow and (16) is valid.

In the next section we will discuss the directional wave spectra and wind buoy observations to be analyzed and how the Stokes drift and wind stress were calculated from the in situ measurements. Then, in section 4, we will use these results to establish that the Stokes drift is essentially in the direction of the local wind.

3. Wind and Directional Wave Spectra Observations and Stokes Drift Calculations

3.1. Buoy Observations

Most of the buoys used were 3-m discus NDBC buoys in the Gulf of Mexico (see Figure 1), but we also included Christmas Island (3-m discus buoy 51028 [0.0°N, 153.913°W]) in the central equatorial Pacific, and

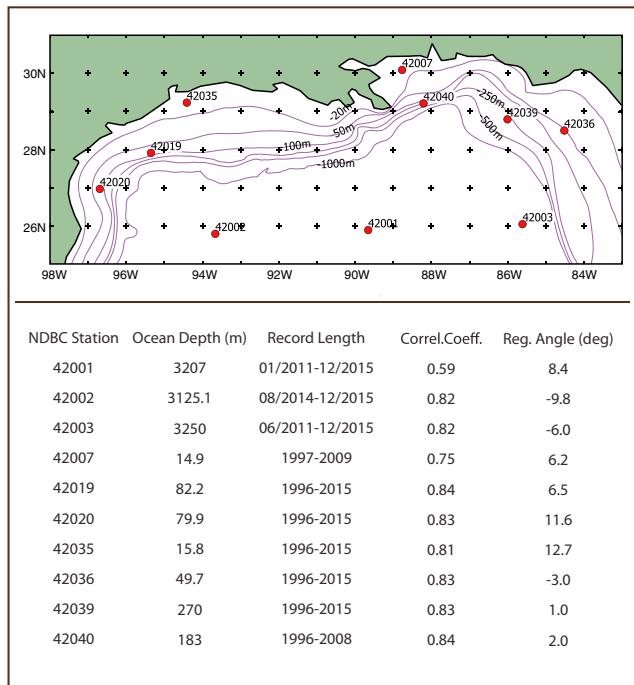


Figure 1. Gulf of Mexico NDBC buoys with long records of simultaneous hourly directional wave spectra and wind measurements. The data beneath the map show the water depth at each buoy, the record length, and the vector correlation between hourly surface Stokes drift and hourly $u \cdot e_w$ at the 10 stations in the Gulf of Mexico (see text). A positive rotation angle means that the Stokes drift vector is rotated to the right of $u \cdot e_w$. Only buoys accurate up to 0.35 Hz were used in the calculations (see text). Although the record length at 42001 is five years, there is only one month of directional wave data. This comparatively small number of data may explain the anomalously low correlation (0.59) there.

Ocean Station Papa (50°N, 150°W) in the North Pacific (see Figure 2). At Ocean Station Papa the wind measurements were made on a buoy separate from the nearby 0.9 m Waverider buoy measurements. Without regard to buoy size, all simultaneous wave and wind records began in 1996 with our calculations ending in 2015 except for 42007 (1997–2009), Christmas Island (1997–2008), and Ocean Station Papa (2010–2015). Further details about the buoy measurements can be found at the websites listed in the Acknowledgments.

The two Pacific stations are affected by remotely driven swell (Snodgrass et al., 1966). Evidence for this in our average spectra is seen by the two-peak spectrum at Christmas Island (see Figure 3).

3.2. Wind Stress Calculations

We calculated the wind stress from the wind measurement heights and hourly wind speed, and wind direction collected by the NDBC and PMEL buoys following Large et al. (1994). The 10-m wind speed u_{10} was adjusted from the wind measurement height to 10 m assuming neutral stability. Given u_{10} , the wind stress $\tau = \rho_a c_D u_{10} \mathbf{u}_{10}$ can be calculated with the neutral drag coefficient (see Appendix A of Large et al., 1994)

$$1000 c_D = 2.70/u_{10} + 0.142 + 0.0764u_{10}. \quad (17)$$

3.3. Stokes Drift Calculations

Simultaneously with the hourly wind observations, hourly buoy wave data were obtained from https://www.ndbc.noaa.gov/historical_data.shtml and <http://cdip.ucsd.edu>. Comparison of directional wave spectra measurements by an Air-Sea Interaction Spar (ASIS) Buoy and a nearby NDBC 3-m discus buoy in the Gulf of Mexico by Drennan et al. (1998) showed that the NDBC directional wave spectra measurements are accurate up to a frequency of 0.35 Hz. Because Stokes drift calculations require knowing the high-frequency part of the spectrum, and because buoys larger than the

3-m discus buoys only resolve frequencies < 0.35 Hz, only the 3-m buoys at the NDBC stations and the smaller wave rider buoy at Ocean Station Papa were used in our calculations. For this reason the data were restricted to the time periods documented in Figure 1. The calculation of Stokes drift from the directional wave spectra is explained in the Appendix A.

4. Relationship Between Surface Stokes Drift and Wind Stress

Past work (Toba, 1973) suggests that the wave spectrum $S(\omega)$ is proportional to the parameter u_* , the square root of the wind stress magnitude $|\tau_0|$ divided by the water density ρ . Since the surface Stokes drift for each ω is proportional to $S(\omega)$, we expect that the magnitude of the Stokes drift will be proportional to u_* and the direction of the Stokes drift will be at some angle to e_w , the unit vector in the direction of the wind. At each buoy for the whole hourly data record we therefore calculated an hourly vector correlation between $u_* e_w$ and Stokes drift vectors estimated as in section 3.

Vector correlations (Figures 1 and 2) for the observed spectrum were all between 0.8 and 0.9 except for three (0.59, 0.75, and 0.77), with Stokes drift rotation ranging from 12.7° to the right of the wind to 9.8° to the left of the wind. Note that the high correlation coefficient for Papa in Figure 2 is consistent with the plot of $|\mathbf{u}_{\text{Stokes}}|$ against u_* in Figure 4b of D'Asaro (2014). Our results are also consistent with the results of two other studies. Ardhuin et al. (2009) deduced from HF radar observations and a numerical wave model that surface Stokes drift and the wind are essentially parallel; Griffin et al. (2016) obtained a similar result using in situ drifter data and Stokes drift estimated from a numerical wave model.

The higher the frequency, the more likely the waves are locally generated and would be in the direction of the wind. We tested this by vectorially correlating $u_* e_w$ with Stokes drift only calculated for the high-

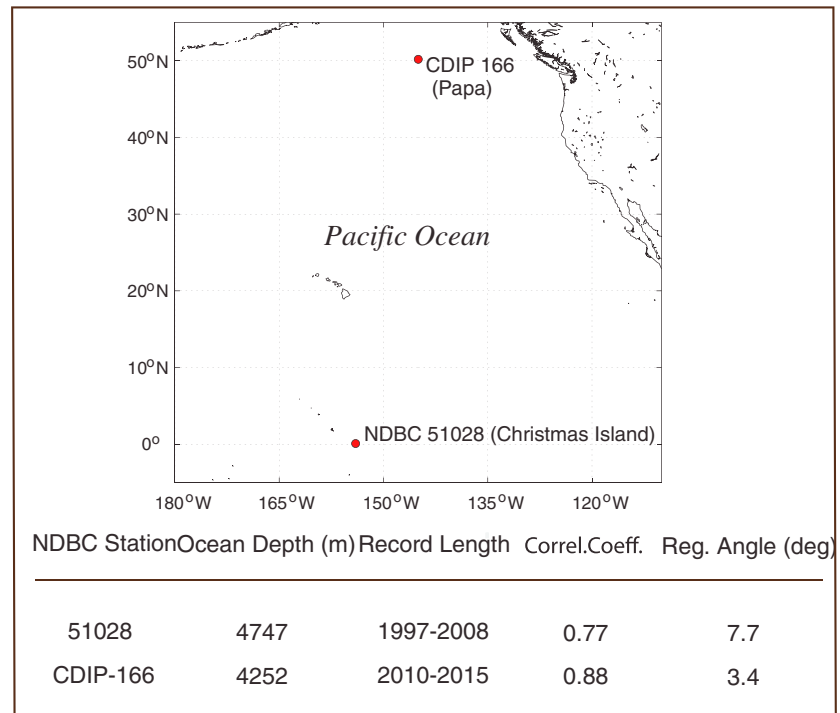


Figure 2. As for Figure 1 but now for the Pacific stations Christmas Island (51028) and Ocean Station Papa (CDIP-166). The Pacific stations are subject to the influence of remotely driven swell, and the average spectrum at Christmas Island (Figure 3) shows clear evidence of this.

frequency band 0.30–0.35 Hz rather than the whole observed spectrum. We found that the angle between the Stokes drift and wind was closer to zero, ranging from 8.4° to the right of the wind to 9.8° to the left. In other words, at the limit of the high frequencies we could resolve, the wind and the Stokes drift were essentially in the same direction and highly correlated; that is, Stokes drift is generated by the local wind stress and is in the direction of the local wind. This is true even for the Pacific stations, including Christmas Island, whose spectrum had two peaks (see Figure 3), the lower frequency peak indicative of remotely driven swell. The vector correlation of 0.77 of local wind stress and Stokes drift at Christmas Island indicates that because of the factor ω^3 , the low-frequency swell does not substantially contribute to the Stokes drift.

If the Stokes drift and local $u_* \mathbf{e}_w$ are highly correlated and, on average in the same direction, how much does the Stokes drift change if we assume that the Stokes drift is always in the wind direction? To answer this question, we compared the time series of $\mathbf{u}_{\text{Stokes}}$ at each of the buoys from the actual data to the Stokes drift calculated assuming that the Stokes drift was always in the wind direction. In the latter case the calculations used the formulation in Appendix A with $r_1(\omega) \equiv 1$ and $\theta_1(\omega)$ always corresponding to the direction of the wind. The results in Table 1 show that the ratio of the average of the Stokes drift speeds at each of the buoys compared to a similar average when the Stokes drift is in the direction of the wind is typically about 70% to 80%. The reduced speed is likely due to wave spreading. Although the local wind and waves are in essentially the same direction *on average*, because of wave spreading, at any given time, the waves and Stokes drift may not be in the direction of the wind and so the component in the direction of the wind will be smaller than the Stokes drift speed. Webb and Fox-Kemper (2015) have taken this into account and suggest that the ratio of the magnitudes depends on $\omega/\omega_{\text{peak}}$, where ω_{peak} is the peak frequency of the spectrum. The ratio of magnitudes is in the range 0.777 to 0.934, but for frequencies $\omega \geq 1.6 \omega_{\text{peak}}$, the ratio is constant and equal to 0.777. These values are comparable to, but slightly larger than, the average ratio of 0.74 in Table 1. Since Stokes drift is dominated by the higher frequencies, the overall effect of wave spreading is likely to reduce the Stokes drift magnitude by a factor at the lower end of the 0.777 to 0.934 range and in what follows we take into account the effect of wave spreading on Stokes drift using the constant factor 0.8.

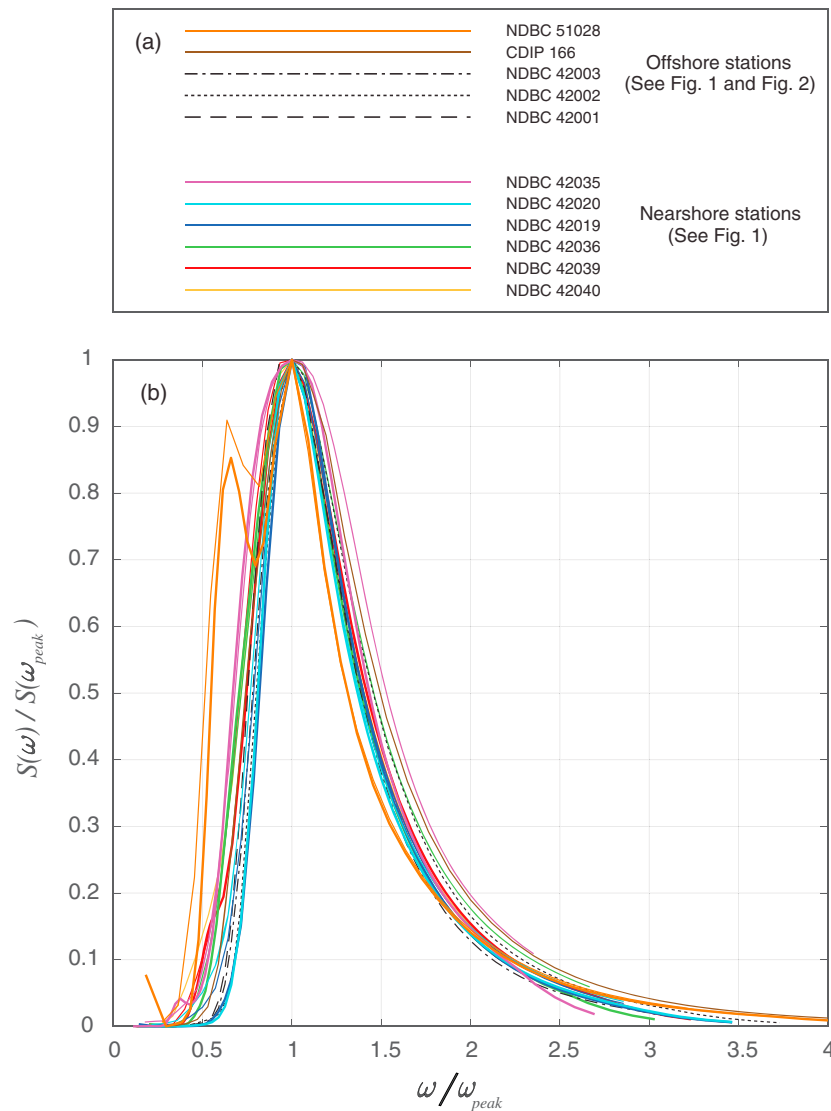


Figure 3. (a) Color code for the buoy station spectra in Figures 1 and 2 and (b) the corresponding averaged spectra. The spectra are nondimensionalized as $S(\omega)/S(\omega_{peak})$ and the frequencies as ω/ω_{peak} . Some buoys have two spectra, one having a thinner line and one a thicker. These represent spectra for different periods of time when the frequency bands changed. The spectra at Christmas Island (NDBC 51028) have two peaks, the lower frequency peak being indicative of remotely forced swell. In order, beginning at NDBC 51028 at the top of the list of stations in (a), the periods in seconds of the peaks of the average spectra at each station are 9.1, 11.8, 7.1, 7.7, 7.1, 5.7, 7.1, 7.1, 6.5, 6.7, and 6.7. The corresponding $S(\omega_{peak})$ in m^2/Hz are 2.4, 9.0, 0.90, 1.0, 0.87, 0.37, 1.2, 1.2, 0.61, 0.75, and 0.77.

5. Extension of the Stokes Drift Analysis to Higher Frequencies

Since the spectrum for locally wind-generated waves depends on g , ω , and u_* , and $S(\omega)$ has the dimensions of length squared multiplied by time, we might expect that $S(\omega)$ would be proportional to $gu_*\omega^{-4}$ consistent with Toba (1973). Our analysis showed that in the high-frequency band, on average, the spectra decayed at slightly less than the expected rate, namely, like ω^{-n} with $n = 3.8 \pm 0.24$. But if $S(\omega)$ goes like ω^{-n} , then since the Stokes drift contribution at frequency ω goes like $\omega^3 S(\omega) d\omega$, it will be proportional to $\omega^{3-n} d\omega$. If the ω^{3-n} decay were to continue, then when the Stokes drift is calculated by integrating over all the frequencies, Stokes drift at the ocean surface would be infinity. Clearly, frequencies higher than we can resolve with buoy data will contribute to the Stokes drift. These higher frequency shorter waves are even more likely to be in the direction of the wind and so contribute to the Stokes drift in

Table 1

At Each Station (Column 1) the Ratio (Column 2) of the Average of the Stokes Drift Speed to the Stokes Drift Speed When the Stokes Drift is Assumed to be in the Direction of the Wind

Station	Ratio of magnitudes
42002	0.72
42003	0.70
42007	0.85
42019	0.73
42020	0.76
42035	0.74
42036	0.75
42039	0.76
42040	0.78
Christmas Island	0.69
Ocean Station Papa	0.68

Note: The first nine entries are in the Gulf of Mexico followed by Christmas Island and Ocean Station Papa in the Pacific. Gulf of Mexico station 42001 has not been included because it only had one month of directional spectra. All calculations used frequencies up to 0.35 Hz.

that direction. But since the surface Stokes drift is not infinity, what brings about a change in the spectral decay?

Phillips (1958) suggested that wave breaking affects the high-frequency behavior. When this occurs the spectrum is no longer dependent on the wind stress and so $S(\omega)$ depends only on ω and g . In this case, by matching the dimensions length squared multiplied by time for $S(\omega)$, it follows that $S(\omega)$ is proportional to $g^2\omega^{-5}$ for large ω and finite surface Stokes drift results. But when does the transition to breaking waves occur?

Waves will break in deep water when they become too steep. The square of the wave steepness $(ka)^2 = 2k^2S(\omega)/d\omega$ integrated up to some frequency ω_{break} is given by

$$I = \int_0^{\omega_{\text{break}}} 2\omega^4 g^{-2} S(\omega) d\omega, \quad (18)$$

where we have used the dispersion relation $k^2 = \omega^4/g^2$. Since $S(\omega)$ at higher frequencies is approximately proportional to $u_*g\omega^{-4}$, at higher frequencies the integrand of I will be approximately constant and I will increase approximately linearly with ω like $u_*\omega/g$ until a critical number $K = u_*\omega_{\text{break}}/g$ when the wave steepness is so large that the waves break.

Forristall (1981) analyzed wave spectra and found that $S(\omega)$ did change from an approximately ω^{-4} to ω^{-5} behavior at a critical frequency. Based on Eq. (14) of Forristall (1981), in our notation

$$K = u_*\omega_{\text{break}}/g = (2\pi)(0.0275)(\rho_{\text{air}}/\rho_{\text{water}})^{1/2} = 0.0061, \quad (19)$$

for air density $\rho_{\text{air}} = 1.2754 \text{ kg/m}^3$ and water density $\rho_{\text{water}} = 1,030 \text{ kg/m}^3$. This value for K is consistent with our analysis of more recent data presented in Figure 2 of Tamura et al. (2014). Note that for realistic u_* the frequency $\omega_{\text{break}} \sim 8$ radians/s corresponds to wavelengths of order a meter, much longer than capillary wavelengths. This justifies the gravity wave dispersion relation in our analysis.

When waves break, Stokes drift no longer operates, and therefore, the Stokes drift estimation ends at the frequency ω_{break} . To include the complete contribution of the waves to the Stokes drift, we must therefore model the directional wave spectrum up to ω_{break} . Our vector correlations showed that to within small error, the wind and Stokes drift up to 0.35 Hz are on average in the same direction. Since this is even more likely for the waves of higher frequency than 0.35 Hz, we assume that all waves that contribute significantly to the Stokes drift propagate in the direction of the wind stress and take into account wave spreading by multiplying by 0.8. It then remains to model the nondirectional spectrum.

For each buoy we estimated the average nondirectional spectrum as a function of u_* up to 0.35 Hz by averaging all the observed spectra in given u_* bins as shown in Figures 4 and 5. For each u_* bin we estimated the spectral decay ω^{-n} of the observed spectrum using the highest eight spectral estimates from 0.28 to 0.35 Hz. We estimated ω^{-n} from 0.35 Hz to ω_{break} by assuming that n increases linearly with ω from its observed value at 0.35 Hz to 5 at $\omega_{\text{break}} = 0.0061 g/u_*$. The spectrum between 0.35 Hz and ω_{break} was thus constructed by using this spectral slope and by matching the observed spectrum at 0.35 Hz. We do not report results for buoy 42002 because there were insufficient data for some u_* and the results for buoy 42007 because it is influenced by land on three sides. Christmas Island (51028) had insufficient data for large u_* , but because it is one of two Pacific stations, we kept it and just plotted valid data.

Figure 4b shows the results for surface u_{Stokes} (u_*) at each buoy, the buoys being color-coded as in Figure 3. First note that for the Gulf of Mexico stations u_{Stokes} (u_*) is larger for buoys nearer the coast than those further offshore. This is likely due to the influence of the fetch; for the same u_* the spectra of buoys nearshore have a higher peak frequency, a greater proportion of higher frequency waves, and hence a larger Stokes drift. Figure 4c shows the average Stokes drift of all the buoys in Figure 4b compared with the average drift of all the buoys not including the extension from 0.35 Hz to $\omega_{\text{break}}/2\pi$. The extension to the wave breaking frequency affects the Stokes drift substantially between the red vertical lines marking the region of typical wind stress. At large u_* the two curves coalesce because for large enough u_* the break frequency $=0.0061 g/u_*$ has

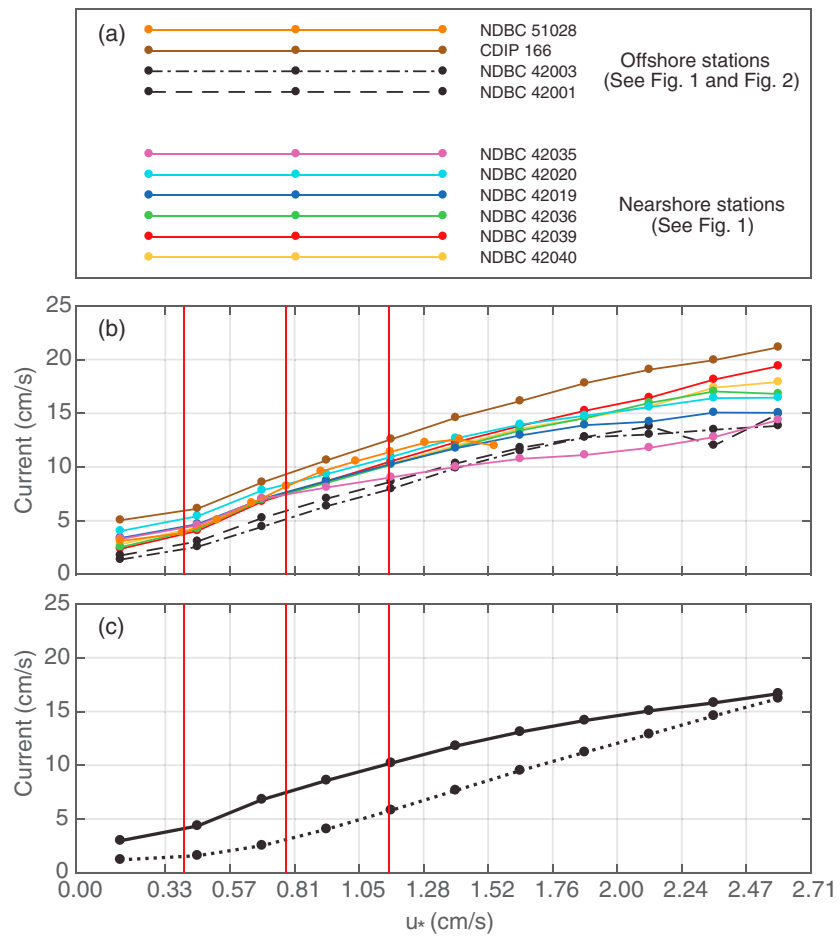


Figure 4. (a) Color codes used in buoy results in (b) and (c). (b) Average surface Stokes drift estimated to ω_{break} . To give some idea of the frequency band in which most of the wind forcing occurs, the red vertical lines correspond to mean $u_* \pm$ one standard deviation. These statistics were calculated as a simple average of the corresponding buoy statistics. (c) Average Stokes drift estimated up to 0.35 Hz (dashed black) compared with the average of all the buoy Stokes drifts calculated up to ω_{break} (solid black).

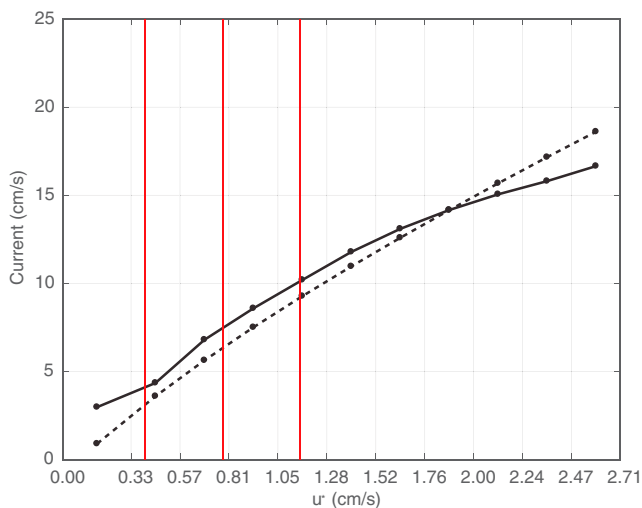


Figure 5. Stokes drift estimate (equation (23)) as a function of u_* (dashed) and Stokes drift averaged over all the buoys (solid as in Figure 4c). The vertical red lines correspond to mean u_* averaged over all buoys \pm one standard deviation.

decreased to $(2\pi)(0.35 \text{ Hz})$ and there is no extension. Finally, note that the Stokes drift significantly affects the movement of surface particles. For example, for a cross-shelf Stokes drift of 10 cm/s, surface particles due to the Stokes drift alone would cross a 100-km-wide shelf in under 12 days. Clearly, it is essential to include the Stokes drift in estimating the movement of oil spills, fish eggs, fish larvae, and toxic red tide blooms to the coast.

6. Results for an Idealized Spectrum

Some simple analytical results can be found using a spectrum based on the Toba (1973) spectral tail

$$S(\omega) = \alpha_{Toba} g u_* (\rho_{water} / \rho_{air})^{1/2} \omega^{-4} \quad (20)$$

but applied for the frequency range $\omega_{peak} \leq \omega \leq \omega_{break}$. In (20) $\alpha_{Toba} = 0.096$ (see Holthuijsen, 2007). For frequencies $\omega > 1.8 \omega_{peak}$ the spectrum (20) is within 10% of the commonly used Donelan et al. (1985)

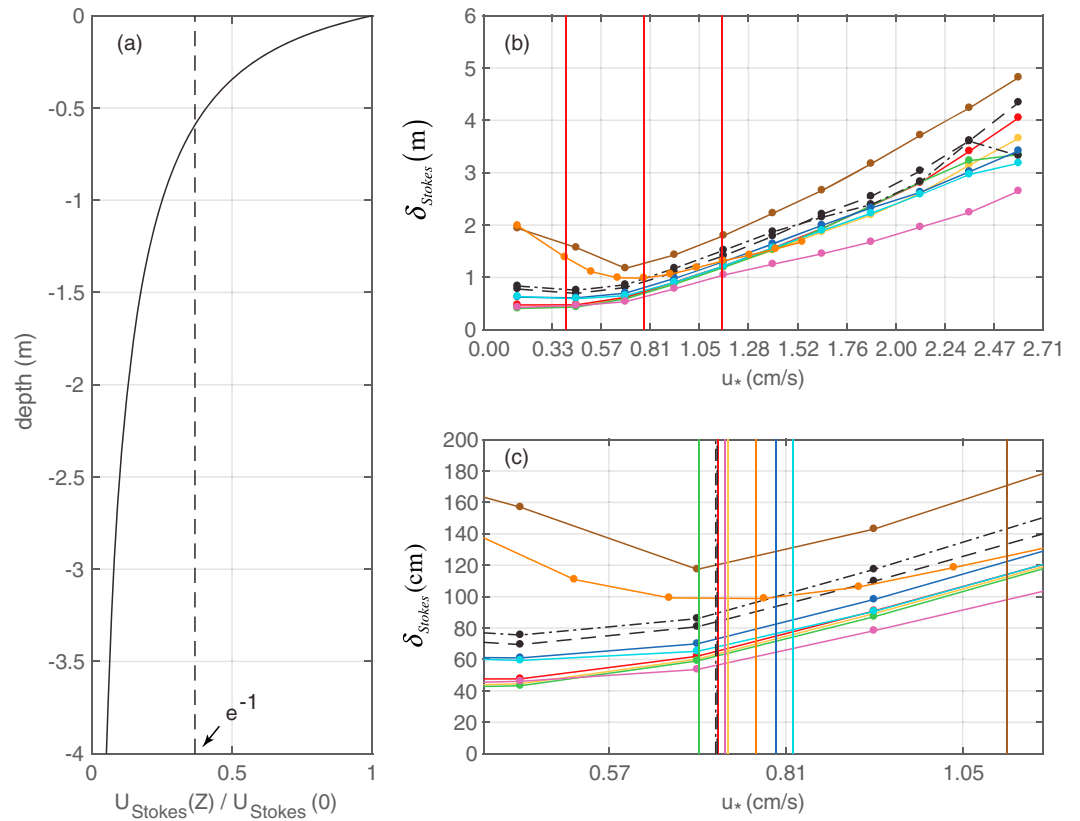


Figure 6. (a) Average Stokes drift speed normalized by the average surface Stokes drift speed at NDBC buoy 42036 (see Figure 1) for the extended spectrum. (b) Average Stokes e-folding scale as a function of u_* for buoys color-coded as in Figure 4a. The red vertical lines mark the mean and standard deviation of u_* averaged over all buoys. (c) Enlargement of (b) between the outside red vertical lines. The vertical colored lines indicate mean u_* for each buoy.

spectrum. For Stokes drift in the direction of the wind, it follows from (1) and (2) that the magnitude of the Stokes drift can be estimated as

$$u_{\text{Stokes}} = (0.8) \int_{\omega_{\text{peak}}}^{\omega_{\text{break}}} 2S(\omega) \omega^3 g^{-1} d\omega, \quad (21)$$

where the factor 0.8 has been included to take into account the effect of wave spreading (see section 5). Substitution of (20) into (21) results in

$$u_{\text{Stokes}} = 1.6 \alpha_{\text{Toba}} u_* (\rho_{\text{water}} / \rho_{\text{air}})^{1/2} \ln(\omega_{\text{break}} / \omega_{\text{peak}}). \quad (22)$$

Using $\omega_{\text{break}} = 0.0061 g/u_*$ and the fully developed sea state peak frequency $\omega_{\text{peak}} = 2\pi g / (7.69 u_{10})$ (Pierson & Moskowitz, 1964) we have

$$u_{\text{Stokes}} = 4.4 u_* \ln(0.0074 u_{10} / u_*). \quad (23)$$

In Figure 5 the result (23) (dashed line) is compared to the Stokes drift averaged over all the buoys (solid line as in Figure 4c). For all but the weakest winds (lowest u_*) and the strongest (two highest u_*), the simple theory Stokes drift differs by only 1 cm/s from the averaged measured Stokes drift. The simple theory curve is almost linear and would be so if the drag coefficient were constant. The decreasing slope for large u_* is due to the Large et al. (1994) drag coefficient's increase as u_{10} increases. For a constant drag coefficient $= 1.2 \times 10^{-3}$, $0.0074 u_{10} / u_* = 6.1$ and consequently $u_{\text{Stokes}} = 7.9 u_*$ or 1.0% of u_{10} . The latter estimate is close to that of the observed drifter and Indian Ocean model analysis of Griffin et al. (2016).

As mentioned earlier, because of wave breaking, we did not include the ω^{-5} part of the spectrum in our estimate. However often used parameterized spectra have an ω^{-5} spectral tail, and for context we decided to compare the Stokes drift estimated for these spectra with ours. The results of Webb and Fox-Kemper (2011), modified to use the same constant drag coefficient 0.0012 and with the 0.8 directional wave spreading factor included, give $u_{\text{Stokes}} = 1.25\% u_{10}$ for the Pierson-Moskowitz spectrum and $0.93\% u_{10}$ for the JONSWAP spectrum. These results are numerically similar to our 1.0% of u_{10} result, but we note that they were obtained under different physical assumptions.

7. Stokes Drift Vertical Decay Scale

For an individual angular frequency ω , the vertical decay scale is $g/(2\omega^2)$, so high frequencies will contribute very small vertical decay scales. Since the high-frequency waves contribute significantly to the Stokes drift, vertical decay scales are very short. Figure 6a shows the average Stokes drift profile at buoy 42036 in the northern Gulf of Mexico (see Figure 1), the Stokes drift being calculated from the extended wave spectrum for the average $u_* = 0.69\text{cm/s}$ at the buoy. Because the vertical profile depends on contributions from many different frequencies, it is not perfectly exponential as for a specific frequency ω . However, it is clear that the vertical decay scale is very short, the Stokes drift profile for average u_* decaying to e^{-1} of its surface value in a vertical scale δ_{Stokes} of only 59 cm, a tiny fraction of the Ekman e -folding scale, which is about 10 m in this region (see, e.g., Maksimova & Clarke, 2013). For $\varepsilon = \delta_{\text{Stokes}}/\delta_{\text{Ek}} = 59\text{ cm}/10\text{ m} \approx 0.059$ it follows from section 2 that the transport of a particle at the surface therefore should be the sum of the Eulerian flow and the Stokes drift. Evidence for such a strong Lagrangian shear in the top 1 m of the water column has been given by Röhrs et al. (2012). In their simultaneous observations of drifters of draft 17 cm and 1 m, when the wind suddenly increased, the shallower drifters immediately moved off in the direction of the wind and waves and separated from the 1 m draft drifters. More recently, experiments by Novelli et al. (2017) using differently drogued near-surface drifters and dye also indicate that there is a very strong near-surface shear.

Figures 6b and 6c show that for the average u_* at each buoy, Christmas Island and 8 stations in the Gulf of Mexico have $\delta_{\text{Stokes}} \leq 1.0\text{ m}$. Ocean station Papa in the North Pacific has a larger $\delta_{\text{Stokes}} = 1.7\text{ m}$ mostly because the average u_* there is much greater than that for the other stations. Note that except for low u_* , δ_{Stokes} at all stations increases with increasing u_* . Physically, as u_* increases, waves break at lower frequencies and so the integration up to ω_{break} extends over a lower frequency range and increases δ_{Stokes} .

The pattern of increasing δ_{Stokes} for increasing u_* is invalid for low u_* , particularly at the two Pacific buoys. At these buoys locally wind-driven Stokes drift is small enough to be affected by the small Stokes drift from remotely driven low-frequency swell. But even at the lowest u_* the e -folding decay scale δ_{Stokes} is only 2 m (Figure 6b).

Other theoretical estimates for Stokes drift profiles and hence deducible δ_{Stokes} have been given based on commonly used parametric spectra (Webb & Fox-Kemper, 2011), observational data but with an ω^{-5} spectral tail (Webb & Fox-Kemper, 2015), or on the results of a third generation wave model (see Breivik et al., 2014, 2016; Tamura et al., 2012). Webb and Fox-Kemper (2015) show an example at ocean station Papa at a particular time where, due to the influence of swell, the Stokes drift profile (see their Figure 4) is strongly influenced by the presence of the swell and extends well below 2 m. However, the third-generation wave model results of Tamura et al. (2012) suggest that on average the δ_{Stokes} decay scale at Papa is 1.9 m. The Tamura et al. (2012) third-generation wave model calculations use a spectral domain extending to 1.05 Hz, a cutoff frequency of comparable size to the variable u_* -dependent cutoff frequencies of section 5. Our δ_{Stokes} for the mean spectrum at Papa (1.7 m) is almost the same as the 1.9 m found by Tamura et al.; our Christmas Island mean δ_{Stokes} (1.0 m) is essentially the same as the Tamura et al. mean (1 m). Furthermore, as mentioned in section 4, the surface Stokes drift is highly correlated with the local wind, indicating that the surface Stokes drift due to the remotely generated swell is typically small compared to locally wind-driven Stokes drift, and therefore does not significantly affect the near-surface Stokes drift and its vertical decay. The Tamura et al. results for the whole north Pacific, coupled with our buoy physically based results with cutoff frequency ω_{break} , suggest that Stokes drift in the direction of the local wind and dominated by short waves with small δ_{Stokes} applies in larger ocean basins than the Gulf of Mexico.

8. Summary and Concluding Remarks

Our results suggest that there is a very thin layer usually less than 1.8 m thick that is key to understanding the transport of surface particles in the ocean. It is directly related to surface waves and the Stokes drift, and because it is thin compared to the Ekman layer depth, it is not canceled by an induced Eulerian flow. The high vector correlations of surface Stokes drift with local wind stress suggest that it is driven by the local wind stress, and the double-peaked Christmas Island spectra suggest that this occurs even when remotely driven swell is present. The surface particle velocity is the Eulerian flow plus $u_{\text{Stokes}}(u_*)\mathbf{e}_w$ where $u_{\text{Stokes}}(u_*)$ is given in Figure 4b.

Our Stokes drift results emphasize the importance of the higher frequency waves and the high-frequency cutoff at ω_{break} where waves break and no longer contribute to the Stokes drift. Consistent with the observed directional spectrum at each buoy, the waves in the extended spectrum between 0.35 Hz and ω_{break} are assumed to be in the direction of the wind with $S(\omega)$ decaying like ω^{-n} and n increasing linearly from its observed value at 0.35 Hz to 5 at ω_{break} . For a given u_* , the Stokes drift is stronger and more vertically sheared nearer the coast where the shorter fetch results in higher frequency waves. Except for the smallest or very large u_* , the simple approximate formula (23) for the surface Stokes drift agrees with the surface Stokes drift averaged over all the estimates to within 1 cm/s.

Our analysis did not consider possible strongly sheared Eulerian flows near the surface and their associated short vertical scales. If the turbulent Ekman layer flow near the surface were to behave like that due to a horizontal rigid wall, there would be a near-surface log layer with very strong shear and short vertical scale as part of the Eulerian Ekman response. Past work by Craig and Banner (1994) showed that there is a wave-enhanced turbulent layer near the surface embedded in a deeper log layer profile. However, δ_{Stokes} is still thin compared to the much thicker Ekman layer beneath the log layer. Thus, even taking into account more realistic near-surface Eulerian flow, ε is still small and we still expect that particle displacement can be approximately found by summing the Eulerian flow and the Stokes drift. Note, however, that the more realistic Eulerian flow should also include a contribution due to the breaking waves that will depend on u_* and will be in the direction of the wind stress. Thus, we can model the surface particle movement by the waveless Eulerian flow plus $(u_{\text{Stokes}} + u_{\text{break}})\mathbf{e}_w$ where the extra Eulerian contribution $u_{\text{break}}\mathbf{e}_w$ is due to breaking waves.

Finally, we note that if realistic near-surface ocean turbulence in the presence of waves is to be understood using large-eddy simulation models, appropriate wave spectra should be used so that the short vertical scales of the Stokes drift near the surface are well represented. Also, a model of particle transport in the real world should take into account both the nonlinear variation of u_{Stokes} with u_* , the fetch nearshore, and limitation of the u_{Stokes} calculation to frequencies less than ω_{break} .

Appendix A: Stokes Drift Calculations From NDBC Directional Wave Spectra

It follows from (2) that if \mathbf{i} is the unit vector in the x (eastward) direction, then the eastward component of the Stokes drift is

$$u_{\text{Stokes}} = \mathbf{u}_{\text{Stokes}} \cdot \mathbf{i} = a^2 \omega^3 g^{-1} \exp(2kz) \cos \theta \quad (\text{A1})$$

given θ is the angle between the unit vectors \mathbf{e}_{wave} and \mathbf{i} . The eastward component of the Stokes drift for the directional wave spectrum $S_{\text{dir}}(\omega, \theta)$ is found by summing the waves over all directions and frequencies, recognizing that $a^2/2 = S_{\text{dir}}(\omega, \theta)d\omega d\theta$. It thus follows from (A1) and the deep water dispersion relation $k = \omega^2/g$ that when integrated over all frequencies and wave directions, the eastward Stokes velocity is

$$u_{\text{Stokes}} = \int_0^\infty \int_0^{2\pi} 2S_{\text{dir}}(\omega, \theta) \omega^3 g^{-1} \exp(2\omega^2 g^{-1} z) \cos \theta d\theta d\omega. \quad (\text{A2})$$

The northward velocity is similarly obtained with $\sin \theta$ replacing $\cos \theta$.

The directional wave spectrum for the NDBC buoys (<https://www.ndbc.noaa.gov/dwa.shtml>) is written in terms of frequencies $\omega/(2\pi)$ but here we keep the angular frequency formulation. The directional spectrum is of the form

$$S_{\text{dir}}(\omega, \theta) = S(\omega)D(\omega, \theta). \quad (\text{A3})$$

In (A3) $S(\omega)$ is the nondirectional spectrum of the waves and $D(\omega, \theta)$ is parameterized as

$$D(\omega, \theta) = \pi^{-1}(0.5 + r_1 \cos(\theta - \theta_1) + r_2 \cos[2(\theta - \theta_2)]), \quad (\text{A4})$$

where $r_1, r_2, \theta_1, \theta_2$ are all functions of the frequency ω . Notice that consistent with $S(\omega)$ being the nondirectional wave spectrum, with $D(\omega, \theta)$ given as in (A4)

$$\int_0^{2\pi} S_{\text{dir}}(\omega, \theta) d\theta = S(\omega). \quad (\text{A5})$$

For the particular form (A3) and (A4), the integral with respect to θ in (A2) can be evaluated analytically to give

$$u_{\text{Stokes}} = \int_0^{\infty} \omega^3 g^{-1} \exp(2\omega^2 g^{-1} z) r_1(\omega) \cos\theta_1(\omega) S(\omega) d\omega. \quad (\text{A6})$$

In practice (A6) and a similar expression for v_{Stokes} with $\sin \theta_1$ replacing $\cos \theta_1$ were evaluated hourly as a finite sum using the hourly values of $S(\omega)$, $r_1(\omega)$, and $\theta_1(\omega)$ obtained from the NDBC records for a finite number of frequencies up to angular frequency $\omega = (2\pi)(0.35) \text{ rad/s}$. We note that $r_1(\omega)$ data at the National Oceanic and Atmospheric Administration website should be normalized by 100 before use and that the National Oceanic and Atmospheric Administration's angle $\alpha_1(\omega) = 270 - \theta_1(\omega)$.

Acknowledgments

We are grateful to David Griffin and other anonymous reviewers whose helpful comments improved our paper, and also to those who gathered decades of hourly buoy data that made our study possible. Funding for this research was provided by the Gulf of Mexico Research Initiative (GoMRI) via the Deep-C Research Consortium (0000022072) SA12-12/GoMRI-008 and the Gulf Research Program of the National Academy of Sciences (2000006432). The content of this publication is solely the responsibility of the authors and does not necessarily represent the official views of the Gulf Research Program or the National Academy of Sciences. The data analyzed in this paper were obtained from the National Data Buoy Center, the Coastal Data Information Program, and the Pacific Marine Environmental Laboratory (https://www.ndbc.noaa.gov/historical_data.shtml), <http://cdip.ucsd.edu> and <https://www.pmel.noaa.gov/ocs/data/disdel>.

References

- Ardhuin, F., Marié, L., Rasclé, N., Forget, P., & Roland, A. (2009). Observation and estimation of Lagrangian, Stokes and Eulerian currents induced by wind and wave at the sea surface. *Journal of Physical Oceanography*, *39*(11), 2820–2838. <https://doi.org/10.1175/2009JPO4169.1>
- Breivik, Ø., Bidlot, J.-R., & Janssen, P. A. E. M. (2016). A Stokes drift approximation based on the Phillips spectrum. *Ocean Modelling*, *100*, 49–56. <https://doi.org/10.1016/j.ocemod.2016.01.005>
- Breivik, Ø., Janssen, P. A. E. M., & Bidlot, J.-R. (2014). Approximate Stokes drift profiles in deep water. *Journal of Physical Oceanography*, *44*(9), 2433–2445. <https://doi.org/10.1175/JPO-D-14-0020.1>
- Craig, P. D., & Banner, M. L. (1994). Modeling wave-enhanced turbulence in the ocean surface layer. *Journal of Physical Oceanography*, *24*(12), 2546–2559. [https://doi.org/10.1175/1520-0485\(1994\)024<2546:MWETIT>2.0.CO;2](https://doi.org/10.1175/1520-0485(1994)024<2546:MWETIT>2.0.CO;2)
- D'Asaro, E. A. (2014). Turbulence in the upper-ocean mixed layer. *Annual Review of Marine Science*, *6*(1), 101–115. <https://doi.org/10.1146/annurev-marine-010213-135138>
- Donelan, M. A., Hamilton, J., & Hui, W. H. (1985). Directional spectra of wind-generated waves. *Philosophical Transactions of the Royal Society of London*, *315*(1534), 509–562. <https://doi.org/10.1098/rsta.1985.0054>
- Drennan, W. M., Graber, H. C., Donelan, M. A., & Terray, E. A. (1998). Directional wave measurements from the ASIS (air-sea interaction spar) buoy. *Oceans '98 Conference Proceedings*, 414–418.
- Forristall, G. W. (1981). Measurement of a saturated range in ocean wave spectra. *Journal of Geophysical Research*, *86*, 8075–8084. <https://doi.org/10.1029/JC086iC09p08075>
- Griffin, D. A., Oke, P. R., & Jones, E. M. (2016). The search for MH370 and ocean surface drift. CSIRO Oceans and Atmosphere, Australia. Report number EP167888. 8 December 2016.
- Hasselmann, K. (1970). Wave-driven inertial oscillations. *Geophysical Fluid Dynamics*, *1*(3-4), 463–502. <https://doi.org/10.1080/03091927009365783>
- Holthuijsen, L. H. (2007). *Waves in oceanic and coastal waters* (p. 387). Cambridge University Press. <https://doi.org/10.1017/CBO9780511618536>
- Large, W. G., McWilliams, J. C., & Doney, S. C. (1994). Oceanic vertical mixing: A review and a model with a nonlocal boundary layer parameterization. *Reviews of Geophysics*, *32*, 363–403. <https://doi.org/10.1029/94RG01872>
- Maksimova, E. V., & Clarke, A. J. (2013). Multiyear subinertial and seasonal Eulerian current observations near the Florida Big Bend coast. *Journal of Physical Oceanography*, *43*(8), 1691–1709. <https://doi.org/10.1175/JPO-D-12-0135.1>
- McWilliams, J. C., Huckle, E., Liang, J.-H., & Sullivan, P. P. (2012). The wavy Ekman layer: Langmuir circulations, breaking waves, and Reynolds stress. *Journal of Physical Oceanography*, *42*(11), 1793–1816. <https://doi.org/10.1175/JPO-D-12-07.1>
- McWilliams, J. C., Sullivan, P. P., & Moeng, C.-H. (1997). Langmuir turbulence in the ocean. *Journal of Fluid Mechanics*, *334*, 1–30. <https://doi.org/10.1017/S00222112096004375>
- Novelli, G., Guigand, C. M., Cousin, C., Ryan, E. H., Laxague, N. J. M., Dai, H., et al. (2017). A biodegradable surface drifter for ocean sampling on a massive scale. *Journal of Atmospheric and Oceanic Technology*, *34*(11), 2509–2532. <https://doi.org/10.1175/JTECH-D-17-0055.1>
- Phillips, O. M. (1958). The equilibrium range in the spectrum of wind-generated waves. *Journal of Fluid Mechanics*, *4*(04), 426–443. <https://doi.org/10.1017/S00222112058000550>
- Pierson, W. J. Jr., & Moskowitz, L. (1964). A proposed spectral form for fully developed wind seas based on the similarity theory of S. A. Kitaigorodskii. *Journal of Geophysical Research*, *69*, 5181–5190. <https://doi.org/10.1029/JZ069i024p05181>

- Pollard, R. T. (1970). Surface waves with rotation: An exact solution. *Journal of Geophysical Research*, *75*, 5895–5898. <https://doi.org/10.1029/JC075i030p05895>
- Polton, J. A., Lewis, D. M., & Belcher, S. E. (2005). The role of wave-induced Coriolis-Stokes forcing of the wind-driven mixed layer. *Journal of Physical Oceanography*, *35*(4), 444–457. <https://doi.org/10.1175/JPO2701.1>
- Röhrs, J., Christensen, K. H., Hole, L. R., Broström, G., Drivdal, M., & Sundby, S. (2012). Observation-based evaluation of surface wave effects on currents and trajectory forecasts. *Ocean Dynamics*, *62*(10-12), 1519–1533. <https://doi.org/10.1007/s10236-012-0576-y>
- Snodgrass, F. E., Groves, G. W., Hasselman, K. F., Miller, G. R., Munk, W. H., & Powers, W. M. (1966). Propagation of ocean swell across the Pacific. *Philosophical Transactions of the Royal Society of London A*, *259*(1103), 431–497. <https://doi.org/10.1098/rsta.1966.0022>
- Stokes, G. G. (1847). On the theory of oscillatory waves. *Transactions of the Cambridge Philosophical Society*, *8*, 441–473.
- Tamura, H., Drennan, W. M., Sahlée, E., & Graber, H. C. (2014). Spectral form and source term balance of short gravity wind waves. *Journal of Geophysical Research: Oceans*, *119*, 7406–7419. <https://doi.org/10.1002/2014JC009869>
- Tamura, H., Miyazawa, Y., & Oey, L.-Y. (2012). The Stokes drift and wave-induced mass flux in the North Pacific. *Journal of Geophysical Research*, *117*, C08021. <https://doi.org/10.1029/2012JC008113>
- Toba, Y. (1973). Local balance in the air-sea boundary processes III. On the spectrum of wind waves. *Journal of the Oceanographic Society of Japan*, *29*(5), 209–220. <https://doi.org/10.1007/BF02108528>
- Ursell, F. (1950). On the theoretical form of ocean swell on a rotating Earth. *Monthly Notices of the Royal Astronomical Society (Geophysical Supplements)*, *6*, 1–8. <https://doi.org/10.1111/j.1365-246X.1950.tb02968.x>
- van den Bremer, T. S., & Breivik, Ø. (2018). Stokes drift. *Philosophical Transactions of the Royal Society*, *376*(2111). <https://doi.org/10.1098/rsta.2017.0104>
- Webb, A., & Fox-Kemper, B. (2011). Wave spectral moments and Stokes drift estimation. *Ocean Modelling*, *40*(3-4), 273–288. <https://doi.org/10.1016/j.ocemod.2011.08.007>
- Webb, A., & Fox-Kemper, B. (2015). Impacts of wave spreading and multidirectional waves on estimating Stokes drift. *Ocean Modelling*, *96*, 49–64. <https://doi.org/10.1016/j.ocemod.2014.12.007>